Eur. Phys. J. B **21**, 31–37 (2001)

THE EUROPEAN PHYSICAL JOURNAL B
EDP Sciences

Unconventional field and angle dependences of the Shubnikov-de Haas oscillations spectra in the quasi two-dimensional organic superconductor $(BEDO\text{-}TTF)_2ReO_4H_2O$

C. Proust[1,a], A. Audouard[1,b], V. Laukhin[2,3], L. Brossard[1], M. Honold[4], M.-S. Nam[4], E. Haanappel[1], J. Singleton[4], and N. Kushch[2]

[1] Laboratoire de Physique de la Matière Condensée[c], Laboratoire National des Champs Magnétiques Pulsés, INSA, 135 avenue de Rangueil, 31077 Toulouse, France
[2] Institute of Problems of Chemical Physics, RAS, Chernogolovka, MD 142432, Russian Federation
[3] Institut de Ciencia de Materiales de Barcelona, Campus de la UAB, 08193 Bellaterra, Spain
[4] University of Oxford, Department of Physics, Clarendon Laboratory, OX1 3PU, UK

Received 22 August 2000 and Received in final form 20 December 2000

Abstract. We report on the inter-layer oscillatory conductance of the two-dimensional organic superconductor $(BEDO\text{-}TTF)_2ReO_4H_2O$ measured in static and pulsed magnetic fields of up to 15 and 52 T, respectively. In agreement with previous in-plane studies, two Shubnikov-de Haas oscillation series linked to the two electron and the hole orbits are observed. The influence of the magnitude and orientation of the magnetic field with respect to the conducting plane is studied in the framework of the conventional two- and three-dimensional Lifshits-Kosevich (LK) model. Deviations of the data from this model are observed in low fields strongly tilted with respect to the normal to the conducting plane. In this latter case, the observed behaviour is consistent with an unexplained lowering of the cyclotron effective mass. At high magnetic field, the oscillatory data could have been compatible with the occurrence of a magnetic breakdown orbit built from the hole and electron orbits. However, the increase of the cyclotron effective mass, linked to the electron orbits, as the magnetic field increases above ~12 T is consistent with a field-induced phase transition. In the lower field range, where the conventional LK model holds, the analysis of the angle dependence of the oscillations amplitude suggests significant renormalisation of the effective Landé factor.

PACS. 71.18.+y Fermi surface: calculations and measurements; effective mass, g factor – 74.70.Kn. Organic superconductors – 72.15.Gd. Galvanomagnetic and other magnetotransport effects

1 Introduction

$(BEDO\text{-}TTF)_2ReO_4H_2O$ is a quasi two-dimensional organic superconductor, which is known to undergo several phase transitions. Indeed, as the temperature is lowered from room temperature, a first order phase transition, corresponding to a reorientation of the ReO_4^- anions, takes place at around 210 K [1–4]. It is also worth to note that water molecules can be removed from crystals under vacuum at room temperature, leading to changes in the crystal structure, with a characteristic time of the order of one day [5]. This phenomenon, which is reversible and frozen at lower temperature, induces significant decrease of the resistivity and suppresses the phase transition at 210 K [6]. As the temperature further decreases another phase transition towards a semimetallic state occurs at a temperature of roughly 30 K [2–4,7–9] (in the following, this phase transition will be referred to as the low temperature phase transition). Finally, the onset of the superconducting transition takes place at around 2 K.

According to band structure calculations based on crystallographic data obtained at a temperature of 170 K [1], *i.e.* below the first order phase transition, Fermi surface (FS) of $(BEDO\text{-}TTF)_2ReO_4H_2O$ is composed of two electron tubes and one hole tube with a cross-sectional area of 2.5 and 5% of the first Brillouin zone (FBZ) area, respectively (see Fig. 1). Magnetoresistance data collected at low magnetic field have revealed two series of Shubnikov-de Haas oscillations, referred to hereafter as S_1 and S_2. Their respective frequencies, F_1 and F_2, correspond to orbit areas of 0.75 and 1.5% of the FBZ area [4,10–12]. Since F_1 is half of F_2, these frequencies have been ascribed to the electron and hole orbits, respectively, although there is a discrepancy by a factor of more than 3 between experimental data and band structure calculations. According to reflectivity data of [9], the

[a] *Present address*: Department of Physics, University of Toronto, 60 St. George Street, Toronto, Ontario M5S 1A7, Canada
[b] e-mail: audouard@insa-tlse.fr
[c] UMR-CNRS 5830

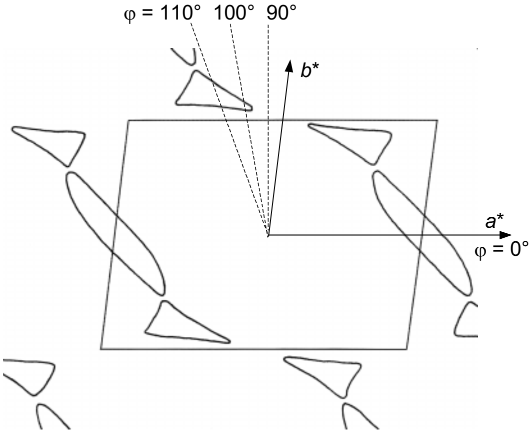

Fig. 1. Fermi surface of (BEDO-TTF)$_2$ReO$_4$H$_2$O at 170 K, according to the band structure calculations of reference [1]. The values of the azimuthal angle φ explored in the reported experiments are indicated.

low temperature phase transition, the nature of which is still not definitely established, could induce some additional changes in the FS topology at lower temperature. However, these changes cannot account for such a large decrease of the orbits' area. Indeed, whereas this phase transition is suppressed by a low hydrostatic pressure (less than 1 kbar) [7], F_1 and F_2 increase continuously only by 7% per kbar [8]. In this context, it should be noted that the discrepancy could originate from the extreme sensitivity of the calculated FS to the value of transfer integrals [13].

A change in the spectrum of the transverse magnetoresistance oscillations has been observed in the higher magnetic field range [11,12]. At magnetic fields higher than $\sim$15 T, the development of oscillations with a frequency F_4 twice F_2 takes place whilst the amplitude A_2 of the S_2 oscillations decreases. In addition, increasing magnetic fields applied parallel to the conducting plane induce a decrease of the transverse magnetoresistance. The attenuation of A_2 with increasing magnetic field was too rapid to be attributable to magnetic breakdown (MB) phenomena only; instead, it has been tentatively ascribed to a field-induced phase transition [11,12].

Investigation of the influence of the orientation of the magnetic field with respect to the conducting plane may yield information on the respective contributions of Zeeman spin splitting and orbital effects to the oscillatory part of the magnetoresistance. A first attempt was presented in reference [12] where only data about the S_2 series could be derived. In addition, most of the above mentioned magnetoresistance experiments were performed on lengthened platelet shaped crystals, for which the current was injected along the most conducting direction a (in-plane configuration). Only a few interlayer magnetoresistance experiments involving short platelet shaped crystals (with the same monoclinic structure as lengthened platelet shaped crystals) have been reported thus far [10]. The aim of this paper is to explore more thoroughly the magnetic field magnitude and orientation dependence of the oscillatory inter-layer magnetoresistance up to high magnetic fields.

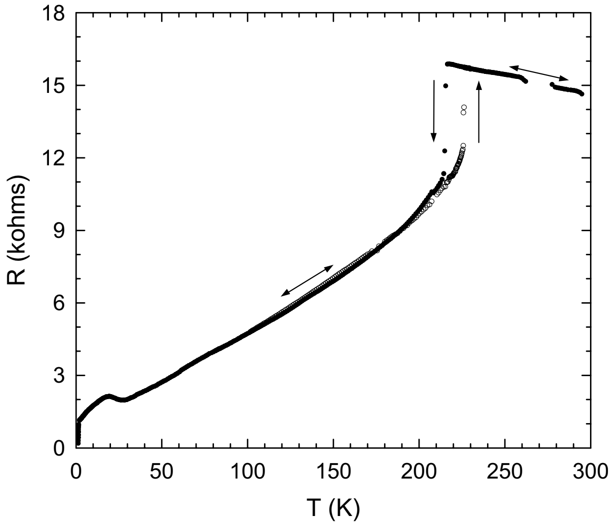

Fig. 2. Temperature dependence of the zero-field interlayer resistance of sample #1 recorded at decreasing (filled circles) and subsequently increasing (empty circles) temperatures.

2 Experimental

The crystals studied were platelets with typical dimensions of $(0.7 \times 0.3 \times 0.05)$ mm^3. The largest faces of the crystals were parallel to the conducting ab-plane and had a parallelogram shape with the longest sides parallel to the a-direction. Magnetoresistance measurements were performed by the standard four-probe method in pulsed magnetic fields of up to 52 T in Toulouse (sample #1) and in static field of up to 15 T in Oxford (sample #2). Electrical contacts were made to the crystals using annealed gold wires of 20 μm in diameter glued with graphite paste. Alternating current (40 μA, 50 kHz and 1 or 10 μA, 333 Hz for pulsed field and static field experiments, respectively) was injected parallel to the c^*-direction. In the following, the orientation of the magnetic field with respect to the crystallographic directions is defined by the angle θ between the field direction and the normal to the conducting ab-plane and by the azimuthal angle φ between the crystallographic a-axis and the projection of the field direction onto the conducting plane (see Fig. 1). For sample #1, the magnetic field was rotated in the plane corresponding to $\varphi = 90°$ while for sample #2, two azimuthal angles were explored, namely $\varphi = 100°$ and $110°$. In order to avoid frozen air within the sample holder at low temperature, the experimental insert was pumped at room temperature before cooling, afterwards helium gas was admitted. As mentioned in the Introduction, water molecules can be extracted from samples by pumping at room temperature. This was prevented by keeping the pumping time at the least ($\sim$1 min). No resistivity change was detected during pumping indicating insignificant water loss.

3 Results and discussion

As shown in Figure 2, the temperature dependence of the inter-layer resistance of sample #1 in zero field displays

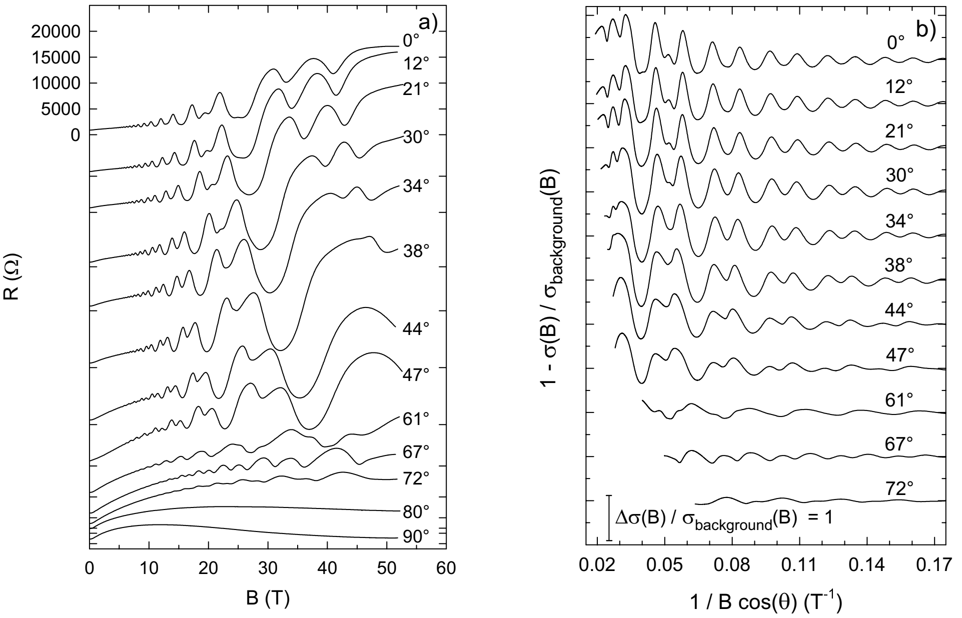

Fig. 3. Field-dependence of the interlayer resistance of sample #1 at 1.7 K and $\varphi = 90°$ for different orientations of the magnetic field (Fig. 3a). The oscillatory part of the conductance derived from the data of Figure 3a and normalised by the monotonic part of the conductance is displayed in Figure 3b.

a hysteretic first order phase transition around 220 K, as already reported [3,7]. As the temperature further decreases, a resistance hump with an onset at 28 K and a maximum at 20 K, due to the low temperature phase transition, is observed. It is worth noting that the hump in the resistance data in Figure 2 has a much smaller amplitude than when measured with the current injected along the a-axis, as mentioned in preliminary investigations [14]. Finally, the onset of superconductivity is observed at 1.5 K.

The inter-layer magnetoresistance of this sample, measured in pulsed fields for $\varphi = 90°$ and for different values of θ, is displayed in Figure 3a. The oscillatory part of the data in Figure 3a, normalised by the field-dependent part of the monotonic conductance is plotted *versus* 1/Bcos(θ) in Figure 3b. Much larger oscillation amplitude (by a factor of 10) and better signal-to-noise ratio than in previous experiments [11,12] are obtained. At present, it is difficult to determine the respective influence of either the configuration of measurement or the sample quality in the observed discrepancy. At low field, the two oscillation series S_1 and S_2, linked to electron and hole orbits are observed. Their respective frequencies, $F_1(\theta = 0) = (39.1 \pm 0.5)$ T and $F_2(\theta = 0) = (77.9 \pm 0.4)$ T, are in agreement with previous magnetoresistance data [4,10–12]. It has been checked that both of the frequencies follow the orbital behaviour expected of quasi-two-dimensional FS sections (*i.e.* $F_i(\theta) = F_i(\theta = 0)/\cos(\theta)$). The value of the frequency ratio $(F_2(\theta)/F_1(\theta) = 1.99 \pm 0.04)$ is in agreement with the picture of a quasi two-dimensional compensated semimetal, as predicted by band structure calculations [1].

In the following, the oscillatory data are analysed in the framework of the conventional Lifshits-Kosevich (LK) model, taking into account the first harmonic of each of the two oscillation series only:

$$\frac{\Delta\sigma}{\sigma} = -\sum_{i=1,2} A_i \cos\left[2\pi\left(\frac{F_i(\theta=0)}{B\cos(\theta)} - \gamma_i\right)\right] \quad (1)$$

where:

$$A_i \propto \frac{T m_{ci}(\theta=0)/\mid B\cos(\theta)\mid^n}{\sinh\mid u_0 T m_{ci}(\theta=0)/B\cos(\theta)\mid} \times \exp\left(-\frac{u_0 T_{Di} m_{ci}(\theta=0)}{\mid B\cos(\theta)\mid}\right)\cos\left|\frac{\pi g_i^* m_{ci}(\theta=0)}{2\cos(\theta)}\right|, \quad (2)$$

m_{ci} is the cyclotron effective mass, g_i^* is the effective Landé spin splitting factor; T_{Di} is the Dingle temperature, γ_i is the Onsager phase factor and u_0 is equal to 14.694 T/K. The exponent n is equal to 1 and 1/2 in the two- and three-dimensional case, respectively. In agreement with Shoenberg [15], this equation assumes that (i) the same cyclotron effective mass m_{ci} is involved in both the spin damping term and the temperature and magnetic field dependence of the oscillation amplitude, (ii) m_{ci} follows the orbital dependence on the field direction expected for a quasi-two-dimensional FS and (iii) the effective Landé spin splitting factor g_i^* is independent on the field direction. At high values of T/B, equation (2) reduces to:

$$A_i \propto \frac{1}{\mid B\cos(\theta)\mid^n}\exp\left(-\frac{\alpha_i}{\mid B\cos(\theta)\mid}\right)\cos\left|\frac{\pi\mu_i}{\cos(\theta)}\right| \quad (3)$$

where $\alpha_i = u_0(T + T_{Di})m_{ci}(\theta = 0°)$ and $\mu_i = g_i^* m_{ci}(\theta = 0°)/2$.

Equation (2) or (3) can be used to derive physical parameters, provided it has been checked that the above

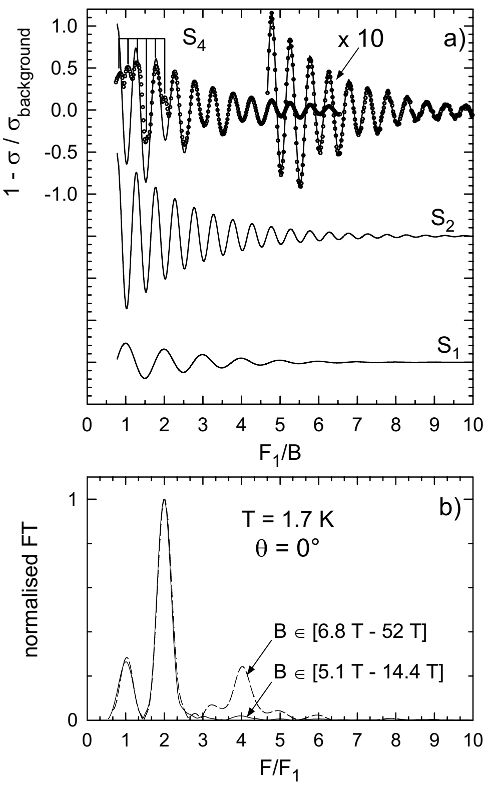

Fig. 4. Oscillatory part of the conductance of sample #1 at 1.7 K and $\theta = 0°$ (Fig. 4a). The upper full line in Figure 4a is the best fit of equations (1) and (2), in the two-dimensional case, to the data in the field range below 14 T. The contribution of the two oscillation series S_1 and S_2 is also shown. Marks labelled S_4 stand for the oscillation series with frequency F_4 (see text). Fourier transforms of the data in Figure 4a are shown in Figure 4b.

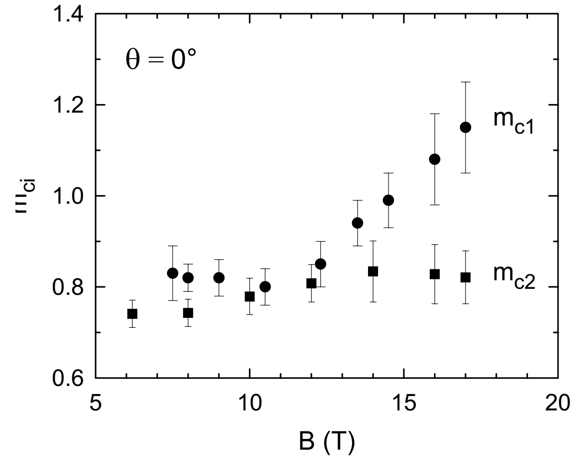

Fig. 5. Magnetic field dependence of the cyclotron effective mass of sample #1 at 1.7 K and $\theta = 0°$ for S_1 and S_2 series.

model accounts for the oscillatory data *versus* temperature and field magnitude and orientation. Note that equation (2) can fail to account satisfactorily for the oscillatory data in good quality crystals of strongly two-dimensional organic compounds, recorded in the high magnetic field and very low temperature ranges. Indeed, under such experimental conditions, the oscillations present a harmonic content larger than predicted by the LK model; furthermore, attempts to derive the cyclotron effective mass from such data can often lead to an apparent field-dependent mass [16].

Figure 4a displays the oscillatory data at $\theta = 0°$. A very good agreement between data and two-dimensional LK model (Eqs. (1) and (2) with $n = 1$) is observed at low magnetic field. By contrast, and in agreement with previously reported analysis of the data in the in-plane configuration of measurements [11,12], some discrepancies appear at high magnetic field (typically, above ∼15 T). In part, these arise from the fact that oscillations with a frequency F_4, twice F_2, appear in the high field range (see Fourier transforms in Fig. 4b). The possible reasons for this behaviour are examined below, through the field and temperature dependence of the oscillation amplitude A_i. In the following, A_i is determined by Fourier transforms (FT) calculated with an elevated cosine window in a given field range from $B_{\min}$ to $B_{\max}$ and is determined by the ratio of the amplitude of the FT to $(1/B_{\min}-1/B_{\max})$.

The cyclotron effective mass has been determined for S_1 and S_2 series in the temperature range 1.5 K to 4.2 K for different mean values of the magnetic field. According to equation (2), two- and three-dimensional LK models yield same values. As displayed in Figure 5, m_{c2} remains almost field-independent ($m_{c2} = 0.75 \pm 0.04$) over the whole magnetic field range covered. Below ∼12 T, m_{c1} is also field-independent ($m_{c1} = 0.82 \pm 0.05$), however, it significantly increases as the magnetic field increases above 12 T.

Figure 6 displays Dingle plots for S_1 and S_2 oscillation series deduced from the data in Figure 3. Solid lines in this figure are best fits to equation (2) for the two-dimensional case. As evidenced in the inset of Figure 6b, a good agreement between the two-dimensional LK model and the data for A_2 is observed up to the highest magnetic fields. In that respect, it must be kept in mind that A_2 is determined through Fourier transforms involving 4 oscillations in the present case, which amounts to a large field window at high field. This point likely hamper the observation of the abrupt, although less pronounced than in the case of previous experimental data [11,12], damping of A_2 evidenced in Figure 4a. Nevertheless, a slight downward deviation of A_2 from the three-dimensional LK model is observed in the inset of Figure 6 at high magnetic field. In this latter case, the damping of A_2, could have been consistent with the development of a MB orbit involving the two electron tubes adjacent to one hole tube. Such a MB orbit should lead to oscillations with a frequency $F_4 = 2F_1 + F_2$ (*i.e.* twice F_2 as displayed in Fig. 4) and to a MB reduction factors $R_{\mathrm{MB1}} = [1 - \exp(-B_0/B)]^{1/2}$ ($R_{\mathrm{MB2}} = [1 - \exp(-B_0/B)]$) for A_1 (A_2) since the electron (hole) orbit involves one (two) Bragg reflections. This assumes that the transmission probability between neighbouring electron orbits is negligible due to the large gap (see Fig. 1). The MB field B_0 deduced from the data at $\theta = 0°$ is of the order of 10–50 T.

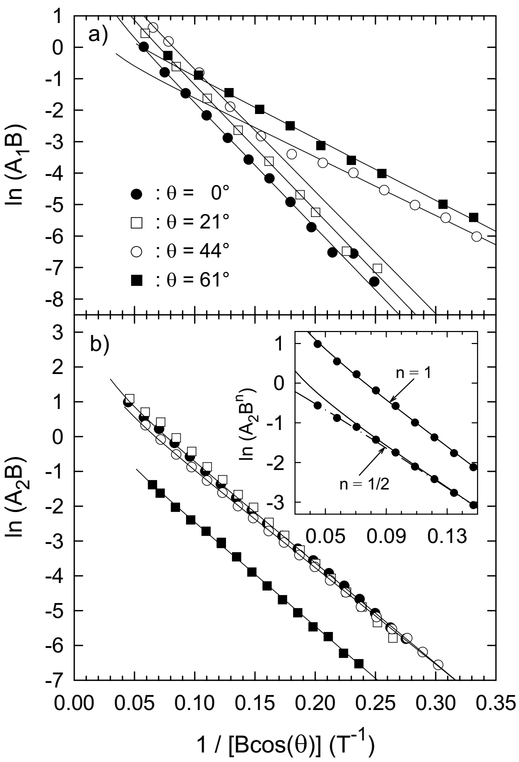

Fig. 6. Dingle plots of the data in Figure 3b for S_1 (Fig. 6a) and S_2 (Fig. 6b) series, in the framework of the two-dimensional model. Full lines are best fits of equation (2) to the data. The inset displays an enlarged view of the data at $\theta = 0°$ in the case of the two- ($n = 1$) and three- ($n = 1/2$) dimensional models. The dash-dotted line is the best fit to the data, including a magnetic breakdown reduction factor with a breakdown field of 30 T (see text).

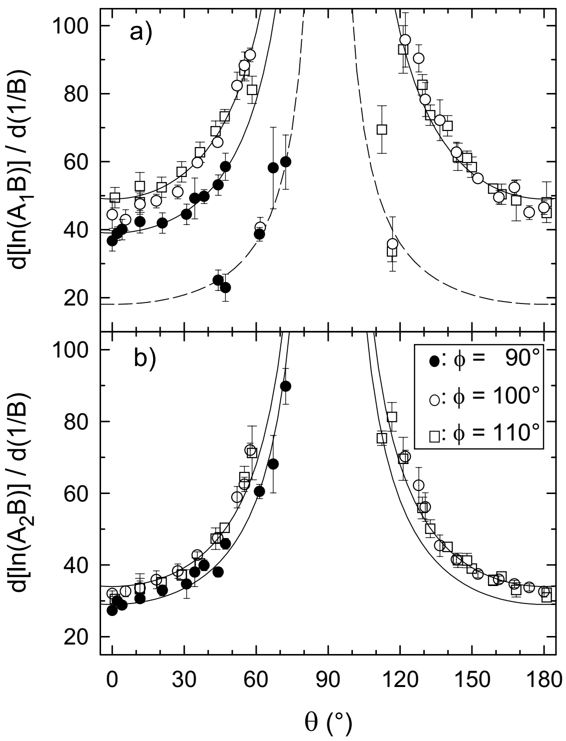

Fig. 7. Angle dependence of d[ln(A_iB)]/d($1/B$) deduced from slopes of Dingle plots of S_1 (Fig. 7a) and S_2 (Fig. 7b) series in the field range where equation (3) accounts for the data. Filled and open symbols correspond to samples #1 and #2, respectively. Lines are best fits of equation (3) to the data. Dashed line in Figure 7a stands for the S_1 series in the high angular range (see text).

Since the reported oscillatory behaviour does not seems to be consistent, in the framework of the two-dimensional LK model, with the development of a MB orbit, a field-induced phase transition is more likely to be considered to account for the data. Indeed, it should be borne in mind that the low temperature semimetallic state of (BEDO-TTF)$_2$ReO$_4$H$_2$O is strongly sensitive to external parameters [7]. Namely, hydrostatic pressure induces a strong increase of m_{c1} in the first few kilobars, followed by a decrease as the pressure further increases, while m_{c2} monotonically decreases *vs.* pressure [8]. In this context, the observed increase of m_{c1} as the magnetic field increases (see Fig. 5) could be the signature of a field-induced phase transition. Nevertheless, several points may hamper reliable data analysis for S_1 oscillation series at high magnetic field. Indeed, (i) the magnetic field magnitude reaches values close to the quantum limit for this series and (ii) the LK model might not describe conveniently the temperature dependence of the oscillation amplitude at high magnetic field, owing to the two-dimensional character of the FS. Regarding point (i), F_1/B indeed goes down to 0.75 at 52 teslas which is within the quantum limit for the S_1 series. However, m_{c1} starts to increase at 12 teslas which corresponds to $F_1/B = 3.3$. In addition, the oscillatory data of charge density wave compounds with small orbit area have been satisfactorily accounted for by the LK model up to magnetic field as large as $B = F/0.63$ and $B = F/0.62$ for KMo$_6$O$_{19}$ and NbSe$_3$, respectively [17]. Deviations from LK model due to the two-dimensional character of the FS (point (ii)) arise when the scattering rate becomes much smaller than the cyclotron frequency, which is actually not the case. In addition, while at low field m_{c1} and m_{c2} have close values and Dingle temperature T_{D2} is significantly lower than T_{D1} (see below), m_{c2} remains field-independent, in agreement with the LK model. The observed variation of m_{c1} could then reflect an actual increase of the cyclotron effective mass.

We will now consider the field range below 12 teslas, in which Dingle plots of Figure 6 are linear, according to equation (3). Regarding oscillation series S_2, good agreement with equation (3) is observed in the whole angular range covered by the experiments and the angle dependence of the slope of the Dingle plots is satisfactorily accounted for by the orbital behaviour predicted by equation (3). This is shown in Figure 6b where data for different values of θ lie on nearly parallel curves. By contrast, the slope of the Dingle plot of the S_1 oscillations at $\theta = 61°$ is much lower than for the data at $\theta = 0°$ and 21° whilst a bend is observed in the field dependence of A_1 at $\theta = 44°$ (see Fig. 6a). These features can also be observed in Figure 7 where the angle dependence of d[ln(A_iB)]/d($1/B$),

Table 1. μ_i values deduced from the angle dependence of the oscillation amplitude and α_i values deduced from magnetic field ($A_i(B)$, see Fig. 7) and angle ($Ai(\theta)$, see Fig. 8) dependence of the oscillation amplitude. α_i and μ_i parameters are defined in equation (3). α_1 values are deduced from the data in the angular range below 60° (see text).

Sample #	φ(°)	α_1 (T)		μ_1	α_2 (T)		μ_2
		A_1(B)	$A_1(\theta)$		A_2(B)	$A_2(\theta)$	
1	90	39.2 ± 1.3	60 ± 12	0.53 ± 0.02	29.5 ± 1.0	71 ± 12	0.55 ± 0.03
2	100	50 ± 4	44 ± 10	0.52 ± 0.01	34 ± 2	50 ± 12	0.54 ± 0.03
2	110	47 ± 3	38 ± 14	0.52 ± 0.02	34 ± 2	39 ± 10	0.58 ± 0.04

deduced from Dingle plots in the low magnetic field range, is displayed for the data collected in pulsed fields (sample #1) and in static fields (sample #2). Lines in this figure are best fits to equation (3). A good agreement is observed in the whole angular range covered by the experiments for A_2 and for θ values lower than ~60° for A_1. The dashed line in the figure is the best fit of equation (3) to the data determined in the high angular range. The α_i values deduced from the fits of the field dependence of A_1 in the angular range below 60° and of A_2 (solid lines in the figure) are given in Table 1. Using the values of the cyclotron effective mass reported above, the deduced Dingle temperatures are $T_{D1} = (1.6 \pm 0.3)$ K [$T_{D1} = (2.5 \pm 0.6)$ K] and $T_{D2} = (1.0 \pm 0.2)$ K [$T_{D2} = (1.3 \pm 0.3)$ K] for sample #1 [#2]. T_D values deduced from the three-dimensional LK model are lower by few tenth of a kelvin when compared to those deduced from the two-dimensional model. In the high angular range, the field dependence of A_1 can be accounted for by $\alpha_1 = (15 \pm 3)$ T. Such a low value can only be interpreted, in the framework of the LK model, by assuming that the cyclotron effective mass is lower for $\theta >\sim 60°$ than for $\theta <\sim 60°$.

Let us now consider the analysis of the angle dependence of the oscillation amplitude, which may yield values of μ_i. In that respect, it is worth recalling that, the conventional LK model has been successfully applied to the analysis of the angle dependence of the oscillation amplitude of several 2D organic conductors such as κ-$(ET)_2Cu(SCN)_2$ [18], α-$(ET)_2TlHg(SCN)_4$ [18], α-$(ET)_2NH_4Hg(SCN)_4$ [18,19], α-$(ET)_2TlHg(SeCN)_4$ [20,21], β-$(ET)_2IBr_2$ [22] or β''-$(ET)_2SF_5CH_2CF_2SO_3$ [23,24]. However, since $F_4(\theta)$ and $F_2(\theta)$ are commensurate to $F_2(\theta)$ and $F_1(\theta)$, respectively, the harmonic ratio procedure, frequently used in order to derive the physical parameters of interest [18,22,25] cannot be used in the present case. Due to the unconventional behaviour of the field dependence of A_1 reported above, the explored angular range was restricted to θ values lower than 60° for the S_1 series. In addition, due to the observed deviations of the data from the LK model at high magnetic field, an intermediate value of the mean field, namely 7.5 T, was considered. As discussed above, the low field approximation of the oscillation amplitude given by equation (3) holds for both series in this field range. Results for samples #1 and #2 are displayed in Figure 8 where solid lines are deduced from the two-dimensional LK model. It has been checked that both two- and three-dimensional LK models account for the data. Contrary to the case of numerous ET salts [19,20,22–24], no clear

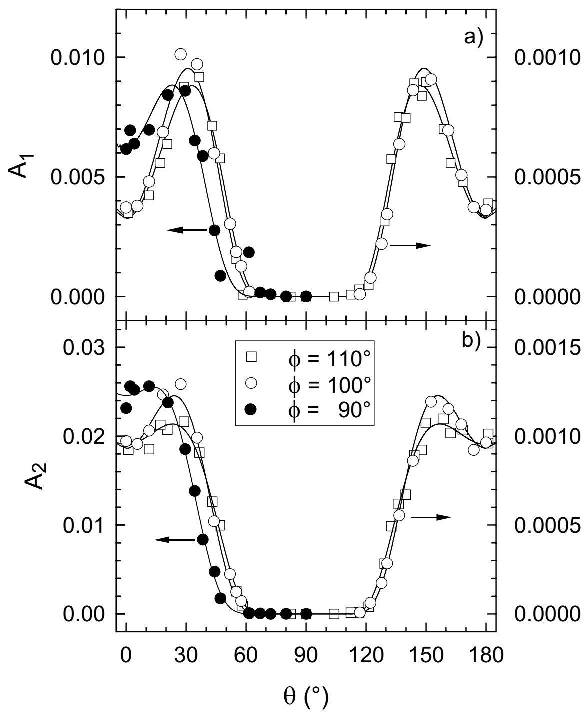

Fig. 8. Angle dependence of the oscillation amplitude for the S_1 (Fig. 8a) and the S_2 (Fig. 8b) series for a mean magnetic field value of 7.5 T. Filled and open symbols correspond to samples #1 and #2, respectively. Full lines are best fits of equation (3) to the data, restricted to the angular range $\theta <$ 60° for the S_1 series.

zero can be observed in Figure 8. As a matter of fact, experimental data for both series cannot be reproduced by using equation (3) if it is assumed that a zero takes place below 60°. This does not allow for μ_i values either in the range 0.25 to 0.5 or larger than 0.75. Solid lines in Figure 8 are best fits to the data, obtained with α_i and μ_i values reported in Table 1. As it is the case for the α_i values deduced from Dingle plots, the three-dimensional LK model yields α_i values lower by few teslas when compared to the two-dimensional model whereas the deduced μ_i values are independent of the model used in the analysis. The large uncertainty of α_i values deduced from the data analysis is due to the lack of sensitivity of the fits to this parameter. It can be noticed that, in some cases (in particular for sample #1), large values of α_i are deduced from the angle dependence of the oscillation amplitude. Similarly, large values of α_i have also been derived in the case of β''-$(ET)_2SF_5CH_2CF_2SO_3$ [23].

For both samples and both oscillation series, μ_i is equal to ca. 0.55 (see Tab. 1) which accounts for the lack of zero in the angle dependence displayed in Figure 8. This value is significantly lower than the cyclotron effective masses linked to each of the oscillation series. This suggests that the effective Landé factor g_i^* is strongly renormalised by interactions as discussed in [15].

4 Conclusion

Most of the features observed in the previous in-plane magnetoresistance data of $(BEDO\text{-}TTF)_2ReO_4H_2O$ are again encountered in the inter-layer magnetoresistance data. In particular, at low magnetic fields perpendicular to the conducting plane, the oscillatory conductance exhibits two oscillations series S_1 and S_2, linked to electron and hole orbits, respectively. The decrease of the amplitude of S_2 oscillations, concomitant with the appearance of an oscillation series with a frequency of twice F_2 at high magnetic field is also detected. Nevertheless, due to a better signal-to-noise ratio in the present case, new features have been observed, mainly regarding S_1 oscillation series. Indeed, while the cyclotron effective mass m_{c2}, linked to the S_2 series remain field-independent, an increase of the cyclotron effective mass m_{c1} is observed as the magnetic field increases above $\sim$12 T. This behaviour is likely to be ascribed to a field-induced phase transition, owing to the fact that pressure-induced increase of m_{c1}, linked to phase transition, have been observed in $(BEDO\text{-}TTF)_2ReO_4H_2O$ [8]. Nevertheless, thermodynamic measurements are needed in order to check this statement.

When the orientation of the magnetic field is changed with respect to the conducting plane, the orbital behaviour of the amplitude of S_2 oscillations, predicted by the Lifshits-Kosevitch model, is observed. As a contrary, the amplitude of S_1 oscillations is larger than predicted for magnetic field strongly tilted with respect to the normal to the conducting plane which could be due to a lowered cyclotron effective mass. Nevertheless, a detailed investigation of this feature is required. In that respect, a systematic study of the field, temperature and angle (both θ and φ) dependences of the oscillatory conductance might be useful. Finally, the analysis of the angle dependence of the oscillation amplitude of both series yield μ_i values (see Eq. (3)) significantly lower than the effective cyclotron mass values. This suggests a significant renormalisation of the effective Landé factor due to interactions.

The authors would like to thank E. Canadell, R.P. Shibaeva and S.S. Khasanov for helpful discussions. S. Askénazy and E.B. Yagubskii are also acknowledged for their support.

References

1. S.S Khasanov, B.Zh. Narymbetov, L.V. Zorina, L.P. Rozenberg, R.P. Shibaeva, N.D. Kushch, E.B. Yagubskii, R. Rousseau, E. Canadell, Eur. Phys. J. B **1**, 419 (1998).
2. S. Kahlich, D. Schweitzer, I. Heinen, S.E. Lan, B. Nuber, H.J. Keller, K. Winzer, H.W. Helberg, Solid State Commun. **80**, 191 (1991).
3. L.I. Buravov, A.G. Khomenko, N.D. Kushch, V.N. Laukhin, A.I. Schegolev, E.B. Yagubskii, L.P. Rozenberg, R.P. Shibaeva, J. Phys I France **2**, 529 (1992).
4. S. Kahlich, D. Schweitzer, C. Rovira, J.A. Paradis, M.-H Whangbo, I. Heinen, H.J. Keller, B. Nuber, P. Bele, H. Brunner, R.P. Shibaeva, Z. Phys. B **94**, 39 (1994).
5. S.S Khasanov, L.V. Zorina, R.P. Shibaeva, N.D. Kushch, E.B. Yagubskii, L.P. Rozenberg, R. Rousseau, E. Canadell, Y. Barrans, J. Gaultier, D. Chasseau, Synth. Met. **103**, 1853 (1999).
6. C. Proust, Ph.D. thesis, University of Toulouse (1999).
7. S. Kahlich, D. Schweitzer, P. Auban-Senzier, D. Jérome, H.J. Keller, Solid State Commun. **83**, 77 (1992).
8. A. Audouard, P. Auban-Senzier, V.N. Laukhin, L. Brossard, D. Jérome, N.D. Kushch Europhys. Lett. **34**, 599 (1996).
9. E. Grießhaber, J. Moldenhauer, D. Schweitzer, I. Heinen, H.J. Keller, W. Strunz, Synth. Met. **87**, 11 (1997).
10. A.E. Kovalev, S.I. Pesotskii, A. Gilevski, N.D. Kushch, J.E.T.P. Letters **59**, 560 (1994) [Pis'ma v Zh. Eksp. Teor. Fiz. **59**, 530 (1994)].
11. A. Audouard, V.N. Laukhin, C. Proust, L. Brossard, N.D. Kushch., J. Phys. France **7**, 599 (1997).
12. A. Audouard, V.N. Laukhin, C. Proust, L. Brossard, N.D. Kushch, S. Askénazy, Physica B **246-247**, 117 (1998)
13. E. Canadell (private communication).
14. C. Proust, A. Audouard, V.N. Laukhin, L. Brossard, M. Honold, M.-S. Nam, E. Haanappel, J. Singleton, N. Kushch, Synth. Met. **103**, 2040 (1999).
15. D. Shoenberg, *Magnetic Oscillations in Metals* (Cambridge University Press, Cambridge, 1984).
16. For a discussion of these problems, which is beyond the scope of the present paper, see *e.g.* I.D. Vagner, T. Maniv, E. Ehrenfreund, Phys. Rev. Lett. **51**, 1700 (1983); and N. Harrison, R. Bogaerts, P.H.P. Reinders, J. Singleton, S.S. Blundell, F. Herlach, Phys. Rev. B **54**, 9977 (1996).
17. A. Rotger, C. Schlenker, J. Dumas, J. Marcus, S. Dubois, A. Audouard, L. Brossard, J.P. Ulmet, S. Askenazy, Synth. Met. **55-57**, 2725 (1993); A. Audouard, J. Richard, S. Dubois, J.P. Ulmet, S. Askénazy, Synth. Met. **55-57**, 2629 (1993).
18. J. Singleton, F.L. Pratt, M. Doporto, J. Caulfield, W. Hayes, I. Deckers, G. Pitsi, F. Herlach, T.J.B.M. Janssen, J.A.A.J. Perenboom, M. Kurmoo, P. Day, Synth. Met. **56**, 2198 (1993).
19. J. Wosnitza, G.W. Crabtree, H.H. Wang, K.D. Carlson, M.D. Vashon, J.M. Williams, Phys. Rev. Lett. **67**, 263 (1991).
20. G. Goll, J. Wosnitza, N.D. Kushch, Europhys. Lett. **35**, 37 (1996).
21. I.J. Lee, V.N. Laukhin, D.K. Petrov, N. Kushch, M.J. Naughton, Synth. Met. **85**, 1559 (1997).
22. J. Wosnitza, *Fermi surfaces of low dimensional organic metals and superconductors* (Springer Verlag, Berlin Heidelberg, New York, 1996).
23. D. Beckmann, S. Wanka, J. Wosnitza, J.M. Williams, P.G. Nixon, R.W. Winter, G.L. Gard, J. Ren, M.-H. Wangbo, Eur. Phys. J. B **1**, 295 (1998).
24. R.E. Edwards, J. Symington, M.-S. Nam, J. Singleton, A. Ardavan, J.E. Schlueter, J. Phys. Cond. Matt. (in press).
25. J. Singleton, Reports on Prog. Phys. **63**, 1111 (2000).